JOURNAL OF GUIDANCE, CONTROL, AND DYNAMICS
Vol. 30, No. 5, September–October 2007

Estimation of Relative Satellite Position Using Transformed Differential Carrier-Phase GPS Measurements

Jonathan D. Wolfe,* Jason L. Speyer,† and Soonsik Hwang‡
University of California, Los Angeles, Los Angeles, California 90095-1597
and
Young Jae Lee§ and Eunsung Lee¶
Konkuk University, Hawyang-Dong Gwangjin-Gu, Seoul 143-701, Republic of Korea

DOI: 10.2514/1.11691

Techniques for applying differential carrier-phase global positioning systems to satellite formation clusters with large (approximately 100 km or more) baselines are described. Because satellites in the cluster may move relative to each other, it is imperative that the carrier-phase ambiguities be resolved quickly and accurately. We propose a transformation of the m-vector carrier-phase measurement equations that restricts the geometric nonlinearities to a one-dimensional subspace and an almost universal linearization of the position state and integer ambiguities in the remaining $m - 1$ dimensional subspace. We then show that all of the measurement equations can be processed with an unscented Kalman filter to quickly compute very accurate floating-point valued estimates of the system state and error covariance. By an integer-preserving transformation found in the least-squares ambiguity decorrelation adjustment method, the number of possible hypotheses for the double-differenced wide-lane ambiguity candidates can be reduced. For the hypotheses set applying a multiple hypothesis Wald sequential probability test, using a specially conditioned form of the transformed global positioning system measurements, quickly and almost optimally determines the correct value of the carrier-phase double-differenced ambiguity. Once the double-differenced wide-lane ambiguities are obtained, the L_1 double-differenced ambiguities are resolved by using L_1 and L_2 carrier-phase measurements based on wide-lane integers in the unscented Kalman filter, then using the least-squares ambiguity decorrelation adjustment method for determining the hypotheses, followed by the multiple hypothesis Wald sequential probability test for resolving the L_1 double-differenced ambiguities. Finally, using the L_1 carrier-phase measurements, the unscented Kalman filter produces the relative position estimates. These techniques are then demonstrated on a simulation of a formation of two satellites in low Earth orbits.

Memorial for Jonathan D. Wolfe **Jon Wolfe first came to my attention through David Chichka, who suggested that a very talented undergraduate student in his orbital mechanics class should join my research group. David's appraisal was excellent, and Jon proved to be a brilliant researcher. At that time, the research group was focused on our joint effort with NASA Dryden and Boeing to develop an automated system for flying aircraft in formation for induced drag reduction, and therefore, reduced fuel consumption. Jon contributed significantly to the understanding of the nonlinear and unstable dynamics that is induced by the trailing vortex off the lead aircraft onto the trailing aircraft. Furthermore, he designed centralized and decentralized controllers for a formation of five aircraft. In particular, his most significant contribution was the development of the instrumentation algorithms to measure the relative distance between two aircraft to the centimeter level in the GPS coordinate frame using differential carrier phase GPS. The essential problem is to resolve the integer ambiguities of the carrier wave. He recognized that by properly annihilating the coefficient matrix of the differential distance and clock bias, the remaining measurement was a linear function of the integers plus noise and, therefore, could be used in the Wald sequential probability hypothesis test to resolve the integers needed in the differential carrier phase measurements. This scheme was tested in flight tests at NASA Dryden on two F-18s, the first demonstration of resolving the integer ambiguities between two moving vehicles, and was shown to be very reliable. The differential carrier phase measurements did produce relative position errors at the centimeter level. In a series of innovative papers, he presented new algorithms for integer resolution, including the current paper. Besides working in differential carrier phase GPS, he made significant contributions to the development of strongly stabilized periodic controllers and target association using detection methods. About four years ago, when Jon was 31, Jon learned that he was very seriously ill. During that time, he remained optimistic about life, cherished his relationships with family and friends, and continued to focus on his career. Throughout this period he remained productive, always insightful and creative, even as he went through painful and extensive treatments. His buoyant and positive attitude showed great courage in the face of adversity. Jon is an inspiration for us all and is greatly missed. Jason L. Speyer**

Presented as Paper 4777 at the AIAA Guidance, Navigation, and Control Conference, Providence, Rhode Island, 16–19 August 2004; received 21 June 2004; revision received 9 January 2007; accepted for publication 28 February 2007.

*Research Engineer, Department of Mechanical and Aerospace Engineering. Member AIAA.
†Professor, Department of Mechanical and Aerospace Engineering. Fellow AIAA.
‡Research Assistant, Department of Aerospace Engineering. Member AIAA.
§Professor, Department of Aerospace Engineering.
¶Researcher, Department of Aerospace Engineering.

Nomenclature

c = speed of light in a vacuum
$\mathbf{I}_{n\times n}$ = the $n \times n$ identity matrix
m = number of global positioning system satellites mutually observed by both stations
$N^{(i)}_{j,L_k}$ = integer ambiguity of station j and global positioning system satellite i for frequency $L_k = L_1, L_2$
$N^{(i)}_{j,\mathrm{WL}}$ = integer ambiguity of station j and global positioning system satellite i for wide-lane combination
$n^{(i)}_j$ = measurement noise associated with $\tilde{\rho}^{(i)}_j$
$\mathbf{S}^{(i)}$ = inertial position of global positioning system satellite i
$\boldsymbol{x}_1$ = inertial position of measurement station 1, expressed as the vector $[x_1 \quad y_1 \quad z_1]^T$
$\boldsymbol{x}_2$ = inertial position of measurement station 2, expressed as the vector $[x_2 \quad y_2 \quad z_2]^T$
$\Delta\tilde{N}^{(i)}$ = integer ambiguity corresponding to $\Delta\tilde{\phi}^{(i)}$
Δt_1 = clock bias between station 1 and global positioning system time
Δt_2 = clock bias between station 2 and global positioning system time
$\Delta\boldsymbol{x}$ = differential position $\boldsymbol{x}_2 - \boldsymbol{x}_1$
$\Delta\tilde{\phi}^{(i)}$ = measured differential carrier phase for the ith global positioning system satellite
$\eta^{(i)}_j$ = measurement noise associated with $\tilde{\phi}^{(i)}_j$
$\eta^{(i)}_{12}$ = measurement noise of the carrier-phase differential measurement $\eta^{(i)}_2 - \eta^{(i)}_1$
$\tilde{\rho}^{(i)}_j$ = measured carrier phase between station $j = 1, 2$ and global positioning system satellite i
$\tilde{\phi}^{(i)}_j$ = measured carrier phase between station $j = 1, 2$ and global positioning system satellite i
χ_d = $\|\boldsymbol{x}_2\|^2 - \|\boldsymbol{x}_1\|^2 + (c\Delta t_1)^2 - (c\Delta t_2)^2$
χ_j = $\|\boldsymbol{x}_j\|^2 - (c\Delta t_j)^2$

I. Introduction

FORMATION flight of satellite clusters has been proposed recently for large-aperture imaging and other applications [1]. The control systems for these clusters would require accurate estimates of the relative positions between the cluster elements. Because the carrier-phase differential global positioning system (GPS) has been used in terrestrial applications to generate very accurate relative position estimates, it is a natural candidate for satellite cluster instrumentation.

Space is an ideal environment for operating differential GPS because a large source of error in terrestrial applications (the difference in the atmospheric conditions above each receiver) is much reduced. There has also been great success in determining the orbits of real-world satellite missions such as TOPEX/POSEIDON, JASON-1, CHAMP, and GRACE using a combination of measurements from onboard GPS receivers and transmissions between GPS ground stations at surveyed locations and the orbiting receivers [2–4]. However, tracking differential positions of *maneuvering* satellite constellations using only onboard GPS receivers and communication between satellites in the formation presents additional problems. In addition to relying on processed GPS measurements from multiple ground stations, conventional GPS precise orbit determination methods are based on smoothing GPS measurements over very long periods. But a formation of satellites may need to maneuver over a short period of time (for instance, to create a new distributed aperture), rapidly changing the orbits of the satellites in the formation.

Autonomous formation flight of spacecraft using GPS instrumentation has been a topic of much interest recently, with researchers reporting accuracies as high as 1.5 mm in relative position during real-time simulations over 4 km baselines [5]. A literature search of six of these claimed successes, reported in [5], revealed that they had all been for baselines of at most 12 km. However, results for a baseline of 200 km using differential carrier-phase GPS measurements and checked with K-band ranging system observations has been reported using level 1 B GRACE GPS observation data [2]. Our results, although simulated, are used to demonstrate the performance of our transformed differential carrier-phase measurements as a possible alternative to the classical linearization approach.

Building upon the estimation techniques that were developed for solving the transformed GPS measurement equations for a single station [6–11], techniques have recently been developed to estimate relative position using transformed differential GPS measurement equations [12]. These transformed GPS measurement equations are obtained by squaring and algebraic manipulations to produce an m set of GPS measurements that can be further decomposed into an $m-1$ universal linear set of measurements and a scalar nonlinear measurement. To extend this approach of constructing universal linear measurements from GPS code measurements to the more accurate carrier-phase measurements requires some nontrivial work. The main contribution of this paper is the derivation of the transformed GPS measurements that include carrier-phase GPS measurements and the validation of their performance in a representative numerical simulation.

The paper is organized as follows: In Sec. II, the main error sources associated with GPS measurements taken by receivers in orbit are discussed. Section III derives the transformed GPS measurement equations for both differential carrier-phase measurements and for absolute measurements between the GPS satellites and the individual receivers. A method for generating floating-point valued estimates of the unknown number of carrier-phase cycles between two receivers with an unscented Kalman filter is discussed in Sec. IV. Note that special emphasis is placed here on quickly generating these estimates, while simultaneously generating estimates of the variance of the estimation error that closely reflect the actual error variance. In Sec. V, an algorithm for resolving first the carrier-phase double-difference wide-lane ambiguities and then the L_1 ambiguities to integer values with a multiple-hypothesis Wald sequential probability test (for ease of presentation, we will subsequently refer to this test simply as the Wald test) is presented. In Sec. VI, the results of the unscented Kalman filter (UKF) estimation procedure for determining very accurate estimates of the relative position between two receivers using double-differenced L_1 carrier-phase measurements is given for a simulation of two receivers in low Earth orbit that are separated by over 100 km. Section VII concludes the paper.

II. Error Sources in GPS Orbital Measurements

To use carrier-phase differential GPS measurements for orbital applications, one must carefully consider the possible contributions of several sources to errors in these measurements. The largest measurement errors found in any GPS measurements are contributed by tropospheric delays, ionospheric effects, ephemeris errors, multipath errors, and by the nonlinear relationship between the user positions and the differential carrier-phase measurements.

Delays caused by propagation of GPS signals through the Earth's troposphere present a particularly difficult problem. The water vapor and dry gases present in the troposphere act to delay signals that travel through the atmosphere close to the Earth [13]. Because of their uniform distribution, the dry constituents of the troposphere affect signal propagation in a predictable way. GPS users at altitudes higher than about 12 km need only consider the well-modeled effects of the dry components of the troposphere. This paper focuses on space applications, in large part, for this reason. Ionospheric refraction can alter the path of the GPS signals significantly as the signals travel from the transmitting satellites to the users [14–16]. Although a large portion of the ionospheric distortion occurs below low Earth orbit (LEO), a still-significant ionospheric delay exists at LEO altitudes. Unfortunately, the best way of mitigating ionospheric effects in GPS requires expensive dual-frequency GPS receivers to estimate or remove first-order ionospheric effects. As a compromise between accuracy and price, we will assume that the receivers used can process coarse/acquisition (C/A) code measurements, as well as both L_1 and L_2 carrier phases (which allows easier integer ambiguity resolution via wide-lane carrier-phase processing). Such receivers are commercially available and are fairly inexpensive, although not as inexpensive as single-frequency receivers. When using these

receivers, some ionospheric distortion must be accepted as unknown biases to the GPS signals, although this effect will not be as strong as the one experienced by Earthbound GPS users.

Differential errors in the GPS broadcast ephemerides can become significant as the baselines between GPS receivers become larger. However, using global precise ephemeris services, such as NASA's Global Differential GPS System which, in operation since 2000, can substantially improve the accuracy of the GPS ephemerides (to the decimeter level).** We assume that our users would subscribe to such a service.

Reflected signals result in multipath error in both code and carrier measurement, even after differencing operation. Multipath has been recognized as a significant factor among other error sources. The strategy to avoid severe multipath error has been introduced. By using proper antenna and adopting cutoff angle or narrow band correlator, the effect of multipath reflection could be mitigated [17]. We assume that multipath delay in measurements is modeled as white Gaussian distribution.

Finally, recall that the GPS measurement equations have a semihyperbolic structure [6–9,12]. For a single GPS user, the user position can be determined by repeated linearization of the measurement equations [7,8]. However, especially in cases where the user position is in orbit, repeated linearization methods can converge to an incorrect solution. We will therefore base our solution method on the measurement equations found in [12] so that their semihyperbolic structure will be taken into proper account.

III. Measurement Equations

To determine the integer ambiguities, we must first make floating-point valued estimates of the system state, including the carrier-phase ambiguities. Once floating-point estimates of sufficient quality are made (as described in Sec. IV), a set of integer-valued candidate hypotheses for the ambiguities can be created. We can then analyze this set of candidate hypotheses with statistical tests to determine the most probable value of the carrier-phase ambiguity. As an initializing Wald test ambiguity searching algorithm, an efficient method of setting searching space is essential for ambiguity problems. Several methods have been developed for reducing the size of the set of candidates that must be considered [18–20]. The least-squares ambiguity decorrelation adjustment (LAMBDA) method is widely used as an ambiguity searching method for its effective aspect of setting searching space. In this paper, as an attempt to reduce the number of test candidates, we will take advantage of only the decorrelation technique, an integer-preserving transformation on the error variance of integer ambiguities to reduce the number of hypotheses, introduced in [18], instead of using the whole LAMBDA procedure. The Wald test is then used to determine the correct integer ambiguities [21].

A. Absolute Pseudorange Measurements

We begin by examining the GPS measurement equation for receiver j corresponding to the ith GPS satellite:

$$\tilde{p}_j^{(i)} = \|\mathbf{S}^{(i)} - \boldsymbol{x}_j\| + ct^{\mathrm{GPS}} - ct_j + n_j^{(i)} \tag{1}$$

where t_j is the clock bias at receiver j, and t^{GPS} is the clock bias between the GPS constellation and the master clock. An equivalent form of Eq. (1) is obtained from the direct method [10]:

$$\begin{aligned} &-2(\mathbf{S}^{(i)})^T\boldsymbol{x}_j + \chi_j + 2\tilde{\rho}_j^{(i)}c\Delta t_j - \left(n_j^{(i)}\right)^2 + 2\tilde{\rho}_j^{(i)}n_j^{(i)} \\ &\quad - 2n_j^{(i)}c\Delta t_j = \left(\tilde{\rho}_j^{(i)}\right)^2 - \|\mathbf{S}^{(i)}\|^2 \end{aligned} \tag{2}$$

where $\chi_j \triangleq \|\boldsymbol{x}_j\|^2 - (c\Delta t_j)^2$. Note that because the elements of the GPS satellite clock offset can be computed, we will write the clock bias particular to receiver j and *all* members of the GPS constellation as $c\Delta t_j \triangleq ct^{\mathrm{GPS}} - ct_j$.

The advantage of the direct method is its rate of convergence to a position estimate. It is shown that the iterative least-square method converges to solution from the center of the Earth with more iteration steps than the iterative direct method [10]. Another benefit is that the initial guessing for an algorithm is not necessary. In case of a semihyperbolic constellation of four satellites, an initial guess not close enough to a solution may not guarantee the correct solution [7]. We can now assemble a vector equation by applying Eq. (2) to the measurements from every satellite that is mutually observed by the two receivers [12]:

$$\mathbf{H}_{jx}\boldsymbol{x}_j + \mathbf{H}_{jj}c\Delta t_j + \mathbf{G}_j\boldsymbol{n}_j + \mathbf{R}_{cj} + \chi_j\mathbf{R}_b = \mathbf{R}_{aj} \tag{3}$$

where

$$\begin{aligned} \mathbf{H}_{jx} &\triangleq 2\begin{bmatrix} -(\mathbf{S}^{(1)})^T \\ -(\mathbf{S}^{(2)})^T \\ \vdots \\ -(\mathbf{S}^{(m)})^T \end{bmatrix}, \qquad \mathbf{H}_{jj} \triangleq 2\begin{bmatrix} \tilde{\rho}_j^{(1)} \\ \tilde{\rho}_j^{(2)} \\ \vdots \\ \tilde{\rho}_j^{(m)} \end{bmatrix} \\ \mathbf{R}_{aj} &\triangleq \begin{bmatrix} \left(\tilde{\rho}_j^{(1)}\right)^2 - \|\mathbf{S}^{(1)}\|^2 \\ \left(\tilde{\rho}_j^{(2)}\right)^2 - \|\mathbf{S}^{(2)}\|^2 \\ \vdots \\ \left(\tilde{\rho}_j^{(m)}\right)^2 - \|\mathbf{S}^{(m)}\|^2 \end{bmatrix} \end{aligned} \tag{4}$$

$$\begin{aligned} \mathbf{G}_j &\triangleq \mathrm{diag}\left\{2\tilde{\rho}_j^{(1)}, 2\tilde{\rho}_j^{(2)}, \ldots, 2\tilde{\rho}_j^{(m)}\right\} \\ \boldsymbol{n}_j &\triangleq \begin{bmatrix} n_j^{(1)} & n_j^{(2)} & \ldots & n_j^{(m)} \end{bmatrix}^T \end{aligned} \tag{5}$$

$$\mathbf{R}_b \triangleq \begin{bmatrix} 1 \\ 1 \\ \vdots \\ 1 \end{bmatrix}, \qquad \mathbf{R}_{cj} \triangleq \begin{bmatrix} -\left(n_j^{(1)}\right)^2 - 2n_j^{(1)}c\Delta t_j \\ -\left(n_j^{(2)}\right)^2 - 2n_j^{(2)}c\Delta t_j \\ \vdots \\ -\left(n_j^{(m)}\right)^2 - 2n_j^{(m)}c\Delta t_j \end{bmatrix} \tag{6}$$

B. Differential Carrier-Phase Measurements

To create the wide-lane precise differential measurements $\delta\tilde{\rho}^{(i)}$, we use L_1 and L_2 differential carrier-phase measurements given as

$$\begin{aligned} \lambda_k\left(\tilde{\phi}_{j,L_k}^{(i)} - \psi_{j,L_k}^{(i)} + \tilde{N}_{j,L_k}^{(i)}\right) &= \|\mathbf{S}^{(i)} - \boldsymbol{x}_j\| + c\delta t_j + \eta_{j,L_k}^{(i)} \\ i = 1, 2, \ldots, m, \qquad j = 1, 2, \qquad k = 1, 2 \end{aligned} \tag{7}$$

where λ_k are the L_1 and L_2 wavelengths, and for every receiver j, a measurement $\tilde{\phi}_{j,L_k}^{(i)}$ at L_k, $k = 1, 2$ frequency of the difference between the phase at the ith GPS satellite vehicle transmitter and the receiver j is made. Note that every carrier-phase measurement $\tilde{\phi}_{j,L_k}^{(i)}$ at receiver j is biased by $\psi_{j,L_k}^{(i)}$, the phase of the local oscillator that generates the carrier-phase replica signal for the carrier-phase tracking loop. In addition to $\tilde{\phi}_{j,L_k}^{(i)} - \psi_{j,L_k}^{(i)}$, an unknown number of full carrier cycles $\tilde{N}_{j,L_k}^{(i)}$ lie between the transmitter and receiver. From L_1 and L_2 measurements, every wide lane observable between the receivers and the transmitters is given by

$$\begin{aligned} \lambda_{\mathrm{WL}}\left(\tilde{\phi}_{j,\mathrm{WL}}^{(i)} - \psi_{j,\mathrm{WL}}^{(i)} + \tilde{N}_{j,\mathrm{WL}}^{(i)}\right) &= \|\mathbf{S}^{(i)} - \boldsymbol{x}_j\| + c\delta t_j + \eta_{j,\mathrm{WL}}^{(i)} \\ i = 1, 2, \ldots, m, \qquad j = 1, 2 \end{aligned} \tag{8}$$

where

***"Broadcast Ephemeris & Almanac" [retrieved 06 July 2006], http://www.gdgps.net/products/broadcast-ephemeris.html.

$$\tilde{N}^{(i)}_{j,\mathrm{WL}} = \tilde{N}^{(i)}_{j,L_1} - \tilde{N}^{(i)}_{j,L_2} \qquad \tilde{\phi}^{(i)}_{j,\mathrm{WL}} = \tilde{\phi}^{(i)}_{j,L_1} - \tilde{\phi}^{(i)}_{j,L_2}$$
$$\lambda_{\mathrm{WL}} = \frac{\lambda_1\lambda_2}{\lambda_2 - \lambda_1} \qquad \psi^{(i)}_{j,\mathrm{WL}} = \psi^{(i)}_{j,L_1} - \psi^{(i)}_{j,L_2}$$
$$\eta^{(i)}_{j,\mathrm{WL}} = \frac{\lambda_2\eta^{(i)}_{j,L_1} - \lambda_1\eta^{(i)}_{j,L_2}}{\lambda_1\lambda_2}$$

and $\eta^{(i)}_{j,\mathrm{WL}}$ is the measurement noise associated with $\tilde{\phi}^{(i)}_{j,\mathrm{WL}}$ in distance units.

We will also assume that the GPS receivers are constructed so that all of the tracking loops at receiver j are in phase with a single carrier-phase replica signal ϕ_{j,L_k} (i.e., $\psi^{(i)}_{j,L_k} = \phi_{j,L_k}, \forall i$). This design practice is fairly common for precision GPS receivers. We will make no corrections for the local oscillator phase bias in the carrier-phase signals, because, as we will show in Sec. V, the carrier-phase measurements can be double differenced by an annihilating projector.

When we take the difference between the wide-lane carrier-phase measurements $\lambda_{\mathrm{WL}}(\tilde{\phi}^{(i)}_{2,\mathrm{WL}} - \phi_{2,\mathrm{WL}} + \tilde{N}^{(i)}_{2,\mathrm{WL}})$ and $\lambda_{\mathrm{WL}}(\tilde{\phi}^{(i)}_{1,\mathrm{WL}} - \phi_{1,\mathrm{WL}} + \tilde{N}^{(i)}_{1,\mathrm{WL}})$, we create a differential measurement

$$\begin{aligned}\delta\tilde{\rho}^{(i)} &\triangleq \lambda_{\mathrm{WL}}\left(\tilde{\phi}^{(i)}_{2,\mathrm{WL}} - \tilde{\phi}^{(i)}_{1,\mathrm{WL}} - \phi_{2,\mathrm{WL}} + \phi_{1,\mathrm{WL}} + \tilde{N}^{(i)}_{2,\mathrm{WL}} - \tilde{N}^{(i)}_{1,\mathrm{WL}}\right)\\ &= \|\mathbf{S}^{(i)} - \boldsymbol{x}_2\| - \|\mathbf{S}^{(i)} - \boldsymbol{x}_1\| + c\Delta t_2 - c\Delta t_1 - \eta^{(i)}_{1,\mathrm{WL}} + \eta^{(i)}_{2,\mathrm{WL}}\end{aligned} \tag{9}$$

To simplify our notation, let us define $\Delta\tilde{N}^{(i)} \triangleq (\tilde{N}^{(i)}_{2,\mathrm{WL}} - \tilde{N}^{(i)}_{1,\mathrm{WL}})$, $\Delta\tilde{\phi}(i) \triangleq (\tilde{\phi}^{(i)}_{2,\mathrm{WL}} - \tilde{\phi}^{(i)}_{1,\mathrm{WL}})$, $\phi_{12} \triangleq \phi_{2,\mathrm{WL}} - \phi_{1,\mathrm{WL}}$, and $\eta^{(i)}_{12} \triangleq (\eta^{(i)}_{2,\mathrm{WL}} - \eta^{(i)}_{1,\mathrm{WL}})$. In the sequel, we will condense our notation by dropping the Δ notation from the carrier-phase differential measurements, and the reader should assume from this point forward that any carrier-phase measurements and any integer ambiguities that we discuss are differential ones. Then, the differential measurement associated with the ith satellite is

$$\begin{aligned}\delta\tilde{\rho}^{(i)} &= \lambda(\tilde{\phi}^{(i)} - \phi_{12} + \tilde{N}^{(i)}) = \|\mathbf{S}^{(i)} - \boldsymbol{x}_2\| - \|\mathbf{S}^{(i)} - \boldsymbol{x}_1\|\\ &\quad + c\Delta t_1 + \eta^{(i)}_{12}\end{aligned} \tag{10}$$

Note that because every phase measurement made at receiver j contains the oscillator phase bias ϕ_j, every differential measurement contains the common-mode bias ϕ_{12}.

Following the procedures in [12], we showed the relationship between the code differential measurement $\delta\tilde{\rho}^{(i)}$ and the L_1 code measurement $\tilde{\rho}^{(i)}_1$ with regard to $\Delta\boldsymbol{x}$.

$$\begin{aligned}&2\boldsymbol{x}_1^T\mathbf{S}^{(i)} - 2\boldsymbol{x}_2^T\mathbf{S}^{(i)} - 2\tilde{\rho}^{(i)}_1 c\Delta t_1 + 2(\tilde{\rho}^{(i)}_1 + \delta\tilde{\rho}^{(i)})c\Delta t_2 - \boldsymbol{x}_1^T\boldsymbol{x}_1\\ &\quad + \boldsymbol{x}_2^T\boldsymbol{x}_2 + (c\Delta t_1)^2 - (c\Delta t_2)^2 + 2\tilde{\rho}^{(i)}_1\eta^{(i)}_{12} + 2\delta\tilde{\rho}^{(i)}\eta^{(i)}_{12}\\ &\quad - 2c\Delta t_2\eta^{(i)}_{12} - \left(\eta^{(i)}_{12}\right)^2 + 2n^{(i)}_1\left[\delta\tilde{\rho}^{(i)} + c\Delta t_1 - c\Delta t_2 - \eta^{(i)}_{12}\right]\\ &\quad = 2\tilde{\rho}^{(i)}_1\delta\tilde{\rho}^{(i)} + (\delta\tilde{\rho}^{(i)})^2\end{aligned} \tag{11}$$

This relationship is true for the code measurement and the differential wide-lane observables introduced in Eq. (10), as well. The only difference is that $\eta^{(i)}_{12}$ is the wide-lane carrier-phase noise and $n^{(i)}_1$ is the same L_1 code noise $\eta^{(i)}_1$ in [12]. Note that differential ambiguity $\tilde{N}^{(i)}$ is included in $\delta\tilde{\rho}^{(i)}_1$ implicitly.

In an analogous way, we can also develop a relationship between the differential carrier-phase measurement $\delta\tilde{\rho}^{(i)}$, the absolute code measurement $\tilde{\rho}^{(i)}_2$, and the states $\boldsymbol{x}_1$, $\boldsymbol{x}_2$, $c\Delta t_1$, $c\Delta t_2$, and $\tilde{N}^{(i)}$:

$$\begin{aligned}&-2\boldsymbol{x}_1^T\mathbf{S}^{(i)} + 2\boldsymbol{x}_2^T\mathbf{S}^{(i)} + 2(\tilde{\rho}^{(i)}_2 - \delta\tilde{\rho}^{(i)})c\Delta t_1 - 2\tilde{\rho}^{(i)}_2 c\Delta t_2 + \boldsymbol{x}_1^T\boldsymbol{x}_1\\ &\quad - \boldsymbol{x}_2^T\boldsymbol{x}_2 - (c\Delta t_2)^2 + (c\Delta t_2)^2 - 2\tilde{\rho}^{(i)}_2\eta^{(i)}_{12} + 2\delta\tilde{\rho}^{(i)}\eta^{(i)}_{12}\\ &\quad + 2c\Delta t_1\eta^{(i)}_{12} - \left(\eta^{(i)}_{12}\right)^2 - 2n^{(i)}_2\left[\delta\tilde{\rho}^{(i)} + c\Delta t_1 - c\Delta t_2 - \eta^{(i)}_{12}\right]\\ &\quad = -2\tilde{\rho}^{(i)}_2\delta\tilde{\rho}^{(i)} + (\delta\tilde{\rho}^{(i)})^2\end{aligned} \tag{12}$$

Note that Eqs. (11) and (12) are forced by a common noise term $\eta^{(i)}_{12}$.

Note that when we add Eqs. (11) and (12) to each other and divide the result by two, the resulting measurement equation has no terms in the states $\boldsymbol{x}_1$ and $\boldsymbol{x}_2$:

$$\begin{aligned}&\left(-\tilde{\rho}^{(i)}_1 + \tilde{\rho}^{(i)}_2 - \delta\tilde{\rho}^{(i)}\right)c\Delta t_1 + \left(\tilde{\rho}^{(i)}_1 + \delta\tilde{\rho}^{(i)} - \tilde{\rho}^{(i)}_2\right)c\Delta t_2\\ &\quad + \left(\tilde{\rho}^{(i)}_1 - \tilde{\rho}^{(i)}_2 + 2\delta\tilde{\rho}^{(i)}\right)\eta^{(i)}_{12} + (c\Delta t_1 - c\Delta t_2)\eta^{(i)}_{12} - \left(\eta^{(i)}_{12}\right)^2\\ &\quad + \left[\delta\tilde{\rho}^{(i)} + c\Delta t_1 - c\Delta t_2 - \eta^{(i)}_{12}\right]\left(n^{(i)}_1 - n^{(i)}_2\right)\\ &\quad = \left(\tilde{\rho}^{(i)}_1 - \tilde{\rho}^{(i)}_2 + \delta\tilde{\rho}^{(i)}\right)\delta\tilde{\rho}^{(i)}\end{aligned} \tag{13}$$

When we subtract (12) from (11) and divide the result by two, we have the measurement equation

$$\begin{aligned}&2\boldsymbol{x}_1^T\mathbf{S}^{(i)} - 2\boldsymbol{x}_2^T\mathbf{S}^{(i)} + \left(-\tilde{\rho}^{(i)}_1 - \tilde{\rho}^{(i)}_2 + \delta\tilde{\rho}^{(i)}\right)c\Delta t_1\\ &\quad + \left(\tilde{\rho}^{(i)}_1 + \delta\tilde{\rho}^{(i)} + \tilde{\rho}^{(i)}_2\right)c\Delta t_2 - \boldsymbol{x}_1^T\boldsymbol{x}_1 + \boldsymbol{x}_2^T\boldsymbol{x}_2 + (c\Delta t_1)^2\\ &\quad - (c\Delta t_2)^2 + \left(\tilde{\rho}^{(i)}_1 + \tilde{\rho}^{(i)}_2\right)\eta^{(i)}_{12} - (c\Delta t_2 + c\Delta t_1)\eta^{(i)}_{12}\\ &\quad + \left[\delta\tilde{\rho}^{(i)} + c\Delta t_1 - c\Delta t_2 - \eta^{(i)}_{12}\right]\left(n^{(i)}_1 + n^{(i)}_2\right)\\ &\quad = \left(\tilde{\rho}^{(i)}_1 + \tilde{\rho}^{(i)}_2\right)\delta\tilde{\rho}^{(i)}\end{aligned} \tag{14}$$

We will use this differential measurement equation in the sequel as the basis for constructing floating-point estimates of $\Delta\boldsymbol{x}$ that are precise enough to reduce the integer ambiguity candidates to a manageable number for integer resolution.

Assembling Eq. (14) for each mutually observed GPS satellite results in the vector measurement equation

$$\begin{aligned}&\mathbf{H}_{dsx1}\boldsymbol{x}_1 + \mathbf{H}_{dsx2}\boldsymbol{x}_2 + \mathbf{H}_{ds1}c\Delta t_1 + \mathbf{H}_{ds2}c\Delta t_2 + \chi_d\mathbf{R}_{bds}\\ &\quad + \mathbf{G}_{ds}\boldsymbol{\eta}_d + \mathbf{R}_{cds} = \mathbf{R}_{ads}\end{aligned} \tag{15}$$

where

$$\mathbf{H}_{dsx1} \triangleq 2\begin{bmatrix}(\mathbf{S}^{(1)})^T\\(\mathbf{S}^{(2)})^T\\\vdots\\(\mathbf{S}^{(m)})^T\end{bmatrix}, \qquad \mathbf{H}_{dsx2} \triangleq \begin{bmatrix}-(\mathbf{S}^{(1)})^T\\-(\mathbf{S}^{(2)})^T\\\vdots\\-(\mathbf{S}^{(m)})^T\end{bmatrix} \tag{16}$$

$$\begin{aligned}\mathbf{H}_{ds1} &\triangleq 2\begin{bmatrix}-\tilde{\rho}^{(1)}_1 - \tilde{\rho}^{(1)}_2 + \delta\tilde{\rho}^{(1)}\\-\tilde{\rho}^{(2)}_1 - \tilde{\rho}^{(2)}_2 + \delta\tilde{\rho}^{(2)}\\\vdots\\-\tilde{\rho}^{(m)}_1 - \tilde{\rho}^{(m)}_2 + \delta\tilde{\rho}^{(m)}\end{bmatrix}\\ \mathbf{H}_{ds2} &\triangleq 2\begin{bmatrix}\tilde{\rho}^{(1)}_1 + \tilde{\rho}^{(1)}_2 + \delta\tilde{\rho}^{(1)}\\\tilde{\rho}^{(2)}_1 + \tilde{\rho}^{(2)}_2 + \delta\tilde{\rho}^{(2)}\\\vdots\\\tilde{\rho}^{(m)}_1 + \tilde{\rho}^{(m)}_2 + \delta\tilde{\rho}^{(m)}\end{bmatrix}\end{aligned} \tag{17}$$

$$\mathbf{G}_{ds} \triangleq \mathrm{diag}\left\{\left(\tilde{\rho}^{(1)}_1 + \tilde{\rho}^{(1)}_2\right), \left(\tilde{\rho}^{(2)}_1 + \tilde{\rho}^{(2)}_2\right), \ldots, \left(\tilde{\rho}^{(m)}_1 + \tilde{\rho}^{(m)}_2\right)\right\} \tag{18}$$

$$\begin{aligned}\mathbf{R}^{(i)}_{cd} &\triangleq (c\Delta t_1 + c\Delta t_2)\eta^{(i)}_{12} + \left[\delta\tilde{\rho}^{(i)} + c\Delta t_1 - c\Delta t_2 - \eta^{(i)}_{12}\right]\\ &\quad \times \left(n^{(i)}_1 + n^{(i)}_2\right)\end{aligned} \tag{19}$$

$$\boldsymbol{\eta}_d \triangleq \begin{bmatrix} \eta_{12}^{(1)} \\ \eta_{12}^{(2)} \\ \vdots \\ \eta_{12}^{(m)} \end{bmatrix}, \qquad \mathbf{R}_{cds} \triangleq \begin{bmatrix} R_{cd}^{(1)} \\ R_{cd}^{2} \\ \vdots \\ R_{cd}^{(m)} \end{bmatrix}, \qquad \mathbf{R}_{bds} \triangleq \begin{bmatrix} 1 \\ 1 \\ \vdots \\ 1 \end{bmatrix}$$

$$\mathbf{R}_{ads} \triangleq \begin{bmatrix} \left(\tilde{\rho}_1^{(1)} + \tilde{\rho}_2^{(1)}\right)\delta\tilde{\rho}^{(1)} \\ \left(\tilde{\rho}_1^{(2)} + \tilde{\rho}_2^{(2)}\right)\delta\tilde{\rho}^{(2)} \\ \vdots \\ \left(\tilde{\rho}_1^{(m)} + \tilde{\rho}_2^{(m)}\right)\delta\tilde{\rho}^{(m)} \end{bmatrix} \tag{20}$$

$$\chi_d \triangleq \chi_2 - \chi_1 \tag{21}$$

C. Simplifying Assumption

Remark: Equations (3) and (15) can be simplified by examining the relative scale of the terms in their expressions [10,12]. For receivers in Earth orbit, typical values for these terms are

$$\|\mathbf{S}^{(i)}\| \approx 10^7 \text{ m}, \qquad \tilde{\rho}_j^{(i)} \approx 10^7 \text{ m}, \qquad c\Delta t_j \approx 10^5 \text{ m}$$
$$n_j^{(i)} \approx \text{m}, \qquad \eta_{12}^{(i)} \approx .1 \text{ m}, \qquad 0 < \|\Delta \boldsymbol{x}\| < 10^5 \text{ m}$$
$$\|\boldsymbol{x}_j\| \approx 10^7 \text{ m}, \qquad 0 < \delta\tilde{\rho}^{(i)} < 10^5 \text{ m}$$

Neglecting terms smaller than 10^7 m^2 in Eq. (3) reduces the measurement equation to

$$\mathbf{H}_{jx}\boldsymbol{x}_j + \mathbf{H}_{jj}c\Delta t_j + \mathbf{G}_j\mathbf{n}_j + \chi_j\mathbf{R}_b = \mathbf{R}_{aj} \tag{22}$$

Similarly, if we neglect terms smaller than 10^6 m^2 in Eq. (15), the differential measurement equation reduces to

$$\mathbf{H}_{dsx1}\boldsymbol{x}_1 + \mathbf{H}_{dsx1}\boldsymbol{x}_2 + \mathbf{H}_{ds1}c\Delta t_1 + \mathbf{H}_{ds2}c\Delta t_2 + \mathbf{G}_{ds}\boldsymbol{\eta}_d + \chi_d\mathbf{R}_{bds} = \mathbf{R}_{ads} \tag{23}$$

The state and the integer ambiguities are linear in Eq. (23) if it is assumed that $\tilde{\rho}_1^{(i)} + \tilde{\rho}_2^{(i)} \gg \delta\tilde{\rho}^{(i)}$ [which is linear in the unknown integer ambiguities, Eq. (10)], e.g.,

$$\frac{\delta\tilde{\rho}^{(i)}}{-\tilde{\rho}_1^{(i)} + \tilde{\rho}_2^{(i)}} \leq 10^{-2} \qquad i = 1, \ldots, m$$

except for the nonlinear term $\chi_d\mathbf{R}_{bds}$. Either $\delta\tilde{\rho}^{(i)}$ can be neglected or replaced by $\tilde{\rho}_2^{(i)} - \tilde{\rho}_1^{(i)}$.

This approach to the universal linearization of the GPS measurements should be contrasted with the linearization for the single difference of Eq. (9) used in [2]. The geometric ranges of each satellite in Eq. (9) are linearized about the absolute position for each satellite. By subtraction, these linearizations are converted to a linear equation composed of the unit line-of-sight vector at satellite 2, times the perturbation along the relative distance plus the difference in the unit line-of-sight vectors at satellite 1 and satellite 2, times the absolute perturbation of the position at satellite 1. If the satellites are close, then the difference in the unit vectors are near zero. If not, the quality of the error in knowing the absolute position needs to be assessed. In [2], the absolute positions of the satellites are very well known.

IV. Filtering Techniques

To generate a candidate set of integer ambiguities, we will first construct a floating-point valued estimate of the carrier-phase ambiguity vector and of its error covariance. Many integer resolution methods have been developed that attempt to efficiently determine the hypothesis set, although none of them have been proven to have optimal efficiency [18–20]. For our tests, we will use the LAMBDA method because it is widely known, with many existing toolkit and library implementations [18]. However, we only use the integer-preserving transformation of the LAMBDA method on the error variance of the integer ambiguities to reduce the number of hypotheses. Thereafter, the Wald test is applied as a sequential nonlinear filter.

In this section, we will develop an estimation filter that quickly yields estimates of sufficient accuracy to generate appropriately sized hypothesis sets that are likely to contain the true value of the integer ambiguity. We will begin the discussion of our estimation filter with a description of the nonlinear dynamic model that it uses. The filter uses the transformed GPS measurements with their universal linear properties.

A. Dynamic model

Our dynamic model of the two-satellite system assumes that both satellites are in elliptical orbits, that the carrier-phase ambiguities are constant over the duration of the filtering process, and that the bias terms $\{c\Delta t_j(t)\}$ of each receiver have second-order dynamics. The state vector for the jth satellite is then taken as

$$\boldsymbol{x}_{\text{state}_j}(t) \triangleq [x_j(t) \quad y_j(t) \quad z_j(t) \quad c\Delta t_j(t) \quad \dot{x}_j(t) \quad \dot{y}_j(t) \quad \dot{z}_j(t) \quad c\dot{\Delta} t_j(t)]^T$$

The dynamic model of each satellite in the two-satellite system is given by the differential equations that describe a satellite motion in an orbit and the second-order differential equation that describes each clock bias. To account for uncertainties present in the system, we introduce process noise terms to the dynamics, generating the nonlinear stochastic differential equations

$$\mathrm{d}x_j(t) = \dot{x}_j(t)\,\mathrm{d}t, \qquad \mathrm{d}y_j(t) = \dot{y}_j(t)\,\mathrm{d}t, \qquad \mathrm{d}z_j(t) = \dot{z}_j(t)\,\mathrm{d}t$$
$$\mathrm{d}(c\Delta t_j)(t) = c\dot{\Delta} t_j(t)\,\mathrm{d}t + \mathrm{d}w_{jt}(t)$$
$$\mathrm{d}\dot{x}_j(t) = -\frac{\mu x_j(t)}{r_j^3(t)}\,\mathrm{d}t + \mathrm{d}w_{j\dot{x}}(t)$$
$$\mathrm{d}\dot{y}_j(t) = -\frac{\mu y_j(t)}{r_j^3(t)}\,\mathrm{d}t + \mathrm{d}w_{j\dot{y}}(t) \qquad \mathrm{d}\dot{z}_j(t) = \frac{\mu z_j(t)}{r_j^3(t)}\,\mathrm{d}t + \mathrm{d}w_{j\dot{z}}(t)$$
$$\mathrm{d}c\dot{\Delta} t_j(t) = \mathrm{d}w_{j\dot{\Delta}t}(t) \tag{24}$$

where μ is the Earth's gravitational constant, $r_j(t) \triangleq \sqrt{x_j(t)^2 + y_j(t)^2 + z_j(t)^2}$ and $w_{jt}(t)$, $w_{j\dot{x}}(t)$, $w_{j\dot{y}}(t)$, $w_{j\dot{z}}(t)$, $w_{j\dot{\Delta}t}(t)$ represent random disturbances. Note that $\mu \triangleq Gm_E$, where G is the universal gravitation constant and m_E is the mass of the Earth. Although μ can be measured directly, m_E must be inferred from μ. It will be convenient in the sequel to write the preceding stochastic differential equations in a vector form:

$$\mathrm{d}\,\boldsymbol{x}_{\text{state}_j}[t, \boldsymbol{w}_j(t)] = \boldsymbol{F}_{\text{sat}}(t, \boldsymbol{x}_{\text{state}_j})\,\mathrm{d}t + \mathrm{d}\boldsymbol{w}_j(t) \tag{25}$$

where $\boldsymbol{F}_{\text{sat}}(t, \boldsymbol{x}_{\text{state}_j})$ is a vector function that describes the dynamics of the elements of $\boldsymbol{x}_{\text{state}}[t, \mathbf{w}_j(t)]$ and $\boldsymbol{w}_j(t) \triangleq [\mathbf{0}_{1\times 3} \quad w_{jt}(t) \quad w_{j\dot{x}}(t) \quad w_{j\dot{y}}(t) w_{j\dot{z}}(t) w_{j\dot{\Delta}t}(t)]^T$.

The carrier-phase ambiguities plus the common-mode phase bias $\{\tilde{N}^{(i)}(t) - \phi_{12}\} \triangleq \{\bar{N}^{(i)}(t)\}$ are assumed to remain constant during the initial filtering stage, and so they are each governed by the differential equation

$$\frac{\mathrm{d}\bar{N}^{(i)}(t)}{\mathrm{d}t} = 0$$

We will assume that every estimated ambiguity in the filter still has uncertainty, therefore, assume that every ambiguity state is corrupted by a small amount of noise. The associated noise variances are tuning parameters that keep the filter open. Then each ambiguity state is

governed by the stochastic differential equation $\mathrm{d}\bar{N}^{(i)}(t) = \mathrm{d}w_{\bar{N}^{(i)}}(t)$, where $\mathrm{d}w_{\bar{N}^{(i)}}(t)$ represents the artificially introduced process noise corresponding to $\bar{N}^{(i)}(t)$.

We can define the ambiguity state vector as

$$\bar{\boldsymbol{N}}_{\text{state}}(t) \triangleq [\,\bar{N}^{(1)}(t) \quad \bar{N}^{(2)}(t) \quad \ldots \quad \bar{N}^{(m)}(t)\,]^T$$

The vector $\bar{\boldsymbol{N}}_{\text{state}}$ is then governed by the vector stochastic differential equation

$$\mathrm{d}\,\bar{\boldsymbol{N}}_{\text{state}}(t) = \mathrm{d}\boldsymbol{w}_{\bar{N}}(t) \tag{26}$$

where $\mathrm{d}\boldsymbol{w}_{\bar{N}}(t) \triangleq [\,\mathrm{d}w_{\bar{N}^{(1)}}(t) \quad \mathrm{d}w_{\bar{N}^{(2)}}(t) \quad \ldots \quad \mathrm{d}w_{\bar{N}^{(m)}}(t)\,]$. Note that if a cycle slip were to occur during the initial filtering stage, the estimation process would be disrupted. Hence, it is very important to resolve the integer ambiguities quickly to minimize the probability that a cycle slip will occur in this critical phase.

We may therefore write the governing stochastic differential equation for the two-satellite system as

$$\mathrm{d}\,\boldsymbol{x}_{\text{state}} = \mathrm{d}\boldsymbol{F}(t, \boldsymbol{x}_{\text{state}}) + \mathrm{d}\boldsymbol{w}(t) \tag{27}$$

where

$$\boldsymbol{x}_{\text{state}}(t) \triangleq \begin{bmatrix} \boldsymbol{x}_{\text{state}_1}(t) \\ \boldsymbol{x}_{\text{state}_2}(t) \\ \bar{\boldsymbol{N}}_{\text{state}}(t) \end{bmatrix}, \qquad \boldsymbol{F}(t, \boldsymbol{x}_{\text{state}}) \triangleq \begin{bmatrix} \boldsymbol{F}_{\text{sat}}(t, \boldsymbol{x}_{\text{state}_1}) \\ \boldsymbol{F}_{\text{sat}}(t, \boldsymbol{x}_{\text{state}_2}) \\ \boldsymbol{0}_{m\times 1} \end{bmatrix}$$

$$\boldsymbol{w}(t) \triangleq \begin{bmatrix} \mathbf{w}_1(t) \\ \mathbf{w}_2(t) \\ \mathbf{w}_{\bar{N}}(t) \end{bmatrix}$$

Because GPS measurements occur at discrete-time intervals, estimation of the states of the two-satellite system requires a discrete-time process model. To generate such a discrete-time model, the process noises are approximated by their integrated values over each GPS epoch, and the equations of motion are numerically integrated over one GPS epoch without noise inputs. The discrete-time process model is then

$$\boldsymbol{x}\,(k)_{\text{state}} \approx \boldsymbol{F}[k-1, \boldsymbol{x}_{\text{state}}(k-1)] + \Gamma_d(k-1)\mathbf{w}(k-1) \tag{29}$$

where $\boldsymbol{F}[k-1, \boldsymbol{x}_{\text{state}}(k-1)] \triangleq \int_{t=(k-1)\tau}^{t=k\tau} \boldsymbol{F}(t, \boldsymbol{x}_{\text{state}})\,\mathrm{d}t$, $\mathbf{w}(k-1) \triangleq \int_{t=(k-1)\tau}^{t=k\tau} \mathbf{w}(t)$, and $\Gamma_d(k-1)$ is obtained by linearizing Eq. (27) about $\boldsymbol{x}(k-1)_{\text{state}}$ and propagating the linearized equation until $t = k\tau$, with $\mathbf{w}(t)$ held constant at $\mathbf{w}(k-1)$.

Using this dynamic model, we will now construct a filter that quickly generates an accurate floating-point valued estimate of the carrier-phase ambiguities and its error covariance.

B. Accurate Nonlinear Filters

Finding an accurate floating-point estimate of the carrier-phase ambiguities and determining the error covariance of this estimate are vital in creating a candidate set that contains the true integer ambiguity and that is sufficiently small. Although the equation describing the system dynamics [Eq. (29)] are nonlinear, the measurement Eqs. (22) and (23) are each linear in the state and integer ambiguities in an $m-1$ dimensional subspace, but the remaining scalar measurement is nonlinear. In attempting to find information relating to the initial carrier-phase ambiguities, we must estimate the entire state space. Our filter design task therefore consists of constructing a filter that can accurately estimate both the first and the second moments of a stochastic process, while simultaneously attempting to reduce the chance of a cycle slip occurring during the estimation process by using as few samples as possible.

Historically, the extended Kalman filter (EKF) has been used for finding floating-point estimates of the carrier-phase ambiguities [16,22,23]. Some aspects of the EKF are problematic. It may diverge and, even when it converges to an accurate value of the mean, it will often generate very poor estimates of the error covariance.

There are several other nonlinear filters that would appear to be better choices than the EKF. A list of possible alternatives to the EKF includes the UKF, the Gauss–Hermite filter, the central difference filter (CDF), and various types of particle filters [24–26]. All of these filters, as well as the EKF, assume that the random variables involved are Bayesian.

Each type of filter attempts to recursively create an estimate $\hat{\mathbf{x}}(k)$ of the current state from the measurement sequence $\mathbf{y}_{1:k} \triangleq \{\mathbf{y}(1), \mathbf{y}(2), \ldots, \mathbf{y}(k)\}$ and the previous state estimate $\hat{\mathbf{x}}(k-1)$ [and the estimated properties of the error associated with $\hat{\mathbf{x}}(k-1)$], given the dynamic system equation

$$\boldsymbol{x}\,(k) = \boldsymbol{F}[\boldsymbol{x}(k-1), \mathbf{w}(k-1)], \qquad \mathbf{y}(k) = \mathbf{H}[\boldsymbol{x}(k), \mathbf{v}(k)] \tag{30}$$

where $\boldsymbol{F}$ and $\mathbf{H}$ are known (nonlinear or linear) functions of the state $\boldsymbol{x}$ and the random processes $\mathbf{w}$ and $\mathbf{v}$. Note that this implies that we wish to construct $p[\boldsymbol{x}(k)|\mathbf{y}_{1:k}]$, the probability density function (PDF) or $\boldsymbol{x}(k)$ given the measurement sequence up to the present time. To accomplish this, each method first seeks to propagate the previous conditional PDF forward in time using the dynamic model and the Chapman–Kolmogorov equation. Then, Bayes' rule can be invoked to incorporate the information in the new measurement $\mathbf{y}(k)$, allowing the construction of the conditional probability $p[\boldsymbol{x}(k)|\mathbf{y}_{1:k}]$. The particle filter, Gauss–Hermite filter, CDF, and UKF differ in the assumptions made about the statistical properties of the noises and in how the sample points that are used to construct sample statistics are chosen. The number of computations required for running a particle filter is much higher than the number required in the other filters. The exponential relationship to state size makes the Gauss–Hermite filter too expensive for our tastes.

Note that when certain assumptions are made about the character of the noises, the UKF and the CDF will create identical estimates. Despite the slight performance advantage of the CDF, we decided to implement our filter as a UKF, because the UKF has a little more flexibility; it relaxes the assumption of a Gaussian distribution and allows for nonadditive noises. Parameters of a UKF can be chosen to capture features of non-Gaussian distributions such as the ones found in Eq. (19) (the skew can be matched and the errors of higher-order moments can be chosen to minimize a quadratic cost function [27]). Another reason that we chose to implement our filter as a UKF is that there is a well-documented square-root implementation of the UKF that can speed up the filtering calculations [28].

This algorithm can be altered slightly to create a square-root version of the UKF [28]. To simplify the discussion, we do not include the square-root algorithm here. However, we recommend that the UKF be implemented with the square-root algorithm in practice, because it enhances the numerical stability and increases the speed of the algorithm.

C. Unscented Kalman Filter Implementation

A floating-point estimate of the state vector $\boldsymbol{x}_{\text{state}}$ suitable for our purposes can be constructed from the two code measurement Eqs. (22), the differential carrier-phase measurement Eq. (23), and the process Eq. (29) using a UKF procedure. For our particular filtering problem, we will assume that the measurement and process noise sequences are zero-mean, Gauss-normal, random variables that are independent in time and uncorrelated with each other. The UKF procedure that we implement for our experiments is the square-root filter described in [28].

We note that a UKF that estimates over the same state space as the one that we have described could be implemented using the measurement Eqs. (1) and (8) instead of the transformed measurement equations. Although this approach has been used successfully [2], the properties of filter convergence using linearized measurements are not well established. In the extreme case, due to poor initialization, such a filter could potentially converge to an erroneous solution, for the same reasons that calculating initial position by repeated linearizations can fail [7,8]. The combination of the transformed measurements and the UKF appear to produce good estimates of the state and integer ambiguities as well as the error

variance of the state and integer ambiguities. Note that in [2], smoothing is used to enhance the estimates of the state and integer ambiguities as well as the error variance of the state and integer ambiguities, which is an offline procedure.

V. Integer Ambiguity Resolution

Although the measurement stations collect differential carrier-phase measurements $\{\tilde{\phi}^{(i)}\}$ (note that these terms include the number of full cycles that pass through the receivers' phase lock loops after they are initialized), the number of full wavelengths between the stations at the beginning of the measurement sequence (the integer ambiguities $\{\tilde{N}^{(i)}\}$) are needed to create the differential carrier-phase measurements $\delta\tilde{\rho}^{(i)} = \lambda(\tilde{\phi}^{(i)} - \phi_{12} + \tilde{N}^{(i)})$, where λ is the wavelength of the GPS carrier signal and ϕ_{12} is the unknown receiver phase difference. To resolve the L_1 frequency ambiguity involves an enormous number of hypotheses that comprise the search space. To reduce the number of hypotheses, we combine the L_1 and L_2 frequencies to produce the wide-lane integer ambiguities. After we ensure the integrity of resolved wide-lane integer ambiguity, the L_1 integer ambiguities are resolved to obtain a more accurate measurement.

Over short baselines, we can take advantage of the linear structure of the corresponding measurement equations and use statistical testing techniques to resolve the integer ambiguities [21]. To adapt this scheme to longer baselines, we shall take advantage of the special structure of our m transformed measurement equations to transform them into $(m-1)$ *linear* equations and a single nonlinear one [12]. We will then operate on the resulting linear equations by additional projections to determine residuals that will be used to determine the carrier-phase integer ambiguities.

First, the double-difference wide-lane integer ambiguities, denoted by the m vector $\boldsymbol{N}$ where the elements of $\boldsymbol{N}$ are $\boldsymbol{N}^{(i)} \triangleq \bar{N}^{(i)} - \bar{N}^{(1)}$, $i = 1, 2, 3, \ldots, m$, are resolved. Note that the first element of $\boldsymbol{N}$ is zero. However, the ambiguities, which are estimated by UKF, are not integer valued. The estimates of $\bar{\boldsymbol{N}}_{\text{state}}(t)$ include the common-mode phase bias. Only the estimate of $c\Delta t_2$ (or, alternatively, the estimate of $c\Delta t_1$) will be affected by substituting $\boldsymbol{N}^{(i)} + \bar{\boldsymbol{N}}^{(i)}$, $i = 1, 2, 3, \ldots, m$ for $\bar{\boldsymbol{N}}$ where the float value of $\bar{\boldsymbol{N}}^{(1)}$ is used. In doing this, we will lose the ability to estimate $c\Delta t_2$ independently of $\tilde{\boldsymbol{N}}^{(1)}$ and ϕ_{12} (or alternatively, we can make a good estimate of $\Delta\boldsymbol{x}$ while only knowing $\boldsymbol{N}$, but lose the ability to estimate $c\Delta t_1$ independently of $\tilde{\boldsymbol{N}}^{(1)}$ and ϕ_{12}.

The residuals used in the Wald test which resolves the double-difference ambiguities $\boldsymbol{N}$ are now constructed. We begin by rewriting measurement Eqs. (1) and (10) as

$$\rho_j^{(i)} \triangleq \tilde{\rho}_j^{(i)} - \left(ct^{\text{GPS}} - ct_j\right) \tag{31}$$

$$\delta\rho^{(i)} \triangleq \delta\tilde{\rho}^{(i)} - (c\Delta t_2 - c\Delta t_1) = \lambda\left(\tilde{\phi}^{(i)} - \phi_{12} + \tilde{N}^{(i)}\right) - (c\Delta t_2 - c\Delta t_1) \tag{32}$$

Substituting Eqs. (31) and (32), following the procedures in [12], gives

$$2\boldsymbol{x}_1^T\mathbf{S}^{(i)} - 2\boldsymbol{x}_2^T\mathbf{S}^{(i)} - \boldsymbol{x}_1^T\boldsymbol{x}_1 + \boldsymbol{x}_2^T\boldsymbol{x}_2 + \left(\rho_1^{(i)} + \rho_2^{(i)}\right)\eta_{12}^{(i)} + \left[\delta\rho^{(i)} - \eta_{12}^{(i)}\right]\left(n_1^{(i)} + n_2^{(i)}\right) = \left(\rho_1^{(i)} + \rho_2^{(i)}\right)\delta\rho^{(i)} \tag{33}$$

For m satellites, the vector form of Eq. (33) is given as

$$\mathbf{H}_{dsx}\Delta\boldsymbol{x} + \chi\mathbf{R}_{bds}\mathbf{G}\boldsymbol{\eta}_d + \mathbf{R}_{cs} = \mathbf{R}_{as} \tag{34}$$

where

$$\mathbf{H}_{dsx} \triangleq -\mathbf{H}_{dsx1}, \qquad \chi \triangleq -\boldsymbol{x}_1^T\boldsymbol{x}_1 + \boldsymbol{x}_2^T\boldsymbol{x}_2 \tag{35}$$

$$\mathbf{G} \triangleq \text{diag}\left\{\left(\rho_1^{(1)} + \rho_2^{(1)}\right), \left(\rho_1^{(2)} + \rho_2^{(2)}\right), \ldots, \left(\rho_1^{(m)} + \rho_2^{(m)}\right)\right\} \tag{36}$$

$$\mathbf{R}_{cs} \triangleq \left[\delta\rho^{(i)} - \eta_{12}^{(i)}\right]\left(n_1^{(i)} + n_2^{(i)}\right) \tag{37}$$

$$\mathbf{R}_{as} \triangleq \mathbf{G}\begin{bmatrix}\delta\rho^{(1)}\\ \delta\rho^{(2)}\\ \vdots\\ \delta\rho^{(m)}\end{bmatrix} \tag{38}$$

Following the simplifying assumption in Sec. III, because the order of $\tilde{\rho}^{(1)} + \tilde{\rho}^{(2)}$ is 10^7 m and the error of estimated $c\Delta t_{12}$ from UKF is less than 10^5 m, $\tilde{\rho}^{(1)} + \tilde{\rho}^{(2)}$ is dominant and $\mathbf{G}^{-1}$ can be approximated by $\mathbf{G}_{ds}^{-1}$. Therefore, multiply Eq. (34) by the matrix $\mathbf{G}_{ds}^{-1}$ to obtain

$$\mathbf{G}_{ds}^{-1}\mathbf{H}_{dsx}\Delta\boldsymbol{x} + \chi_d\mathbf{G}_{ds}^{-1}\mathbf{R}_{bds} + \mathbf{G}_{ds}^{-1}\mathbf{G}\boldsymbol{\eta}_d = \mathbf{G}_{ds}^{-1}\mathbf{G}\delta\rho \tag{39}$$

where $\delta\rho = \lambda(\phi + N) + \mathbf{R}_{bds}[\lambda(\phi_{12} + \tilde{N}^{(1)}) + c\Delta t_{12}]$ and

$$\tilde{\phi} + N = [\tilde{\phi}^{(1)} + 0, \tilde{\phi}^{(2)} + N^{(2)}, \ldots, \tilde{\phi}^{(m)} + N^{(m)}]^T$$

A projector $\mathbf{E}$ is constructed such that $\mathbf{E}\mathbf{R}_{bds} = 0$ and eliminates the term $\mathbf{R}_{bds}[\lambda(\phi_{12} + \tilde{N}^{(1)}) + c\Delta t_{12}]$ in $\delta\rho$. Note that the projector $\mathbf{E}$ induces double differences in the integers. Essentially, the projection forms the double-difference effects by subtracting the single difference measurements from each other. A second projector $\mathbf{E}_d$ is constructed such that $\mathbf{E}_d\mathbf{E}\mathbf{G}_{ds}^{-1}\mathbf{R}_{bds} = 0$ and eliminates the nonlinearity. Clearly, to a large degree, the construction of these projectors and the order they are applied are arbitrary. Applying these projectors, Eq. (39) becomes

$$\mathbf{E}_d\mathbf{E}\mathbf{G}_{ds}^{-1}\mathbf{H}_{dsx}\Delta\boldsymbol{x} + \mathbf{E}_d\mathbf{E}\eta_d = \mathbf{E}_d\mathbf{E}[\tilde{\phi} + N] \tag{40}$$

If the term involving $\Delta\boldsymbol{x}$ is annihilated by the projector $\mathbf{E}_H$ as $\mathbf{E}_H\mathbf{E}_d\mathbf{E}\mathbf{G}_{ds}^{-1}\mathbf{H}_{dsx} = 0$, the residual for the Wald test becomes

$$\mathbf{r}_{\mathbf{carrier}_j} \triangleq \mathbf{E}_H\mathbf{E}_d\mathbf{E}\eta_d = \mathbf{E}_H\mathbf{E}_d\mathbf{E}[\tilde{\phi} + N_j] \tag{41}$$

where the subscript j in the vector $\mathbf{r}_{\mathbf{carrier}_j} \in \mathbb{R}^{m-5}$ refers to the jth hypotheses. Furthermore, this residual has uncertainty at the level of the carrier-phase noise. However, to enhance performance of the Wald test, additional double-difference residuals are constructed as

$$\mathbf{r}_{\mathbf{code}_j} \triangleq [\lambda(\nabla\tilde{\phi} + \check{N}_j) - \nabla\Delta\tilde{\rho}] \in \mathbb{R}^{m-1} \tag{42}$$

where $\nabla\tilde{\phi}$ is double-difference phase measurements, $\nabla\Delta\tilde{\rho}$ is double-difference code measurements, and $\check{N}_j$ is an $m-1$ vector representing all the elements of N_j but the first. This residual, $\mathbf{r}_{\mathbf{code}\,j}$ has uncertainty at the level of code noise.

Algorithm (Wald test):

1. Choose a threshold value T for the probability that a particular set of integers is the correct one. This is the stopping criterion for the test.
2. Generate floating-point valued estimates of $\{\bar{N}^{(i)}\}$ as $\{\hat{\bar{N}}^{(i)}\}$ using the techniques discussed in Sec. IV.
3. Choose a collection of sets of possible hypotheses that differ by integer values from each other and that are near to the floating-point estimates. Using, for instance, an integer-preserving transformation from the LAMBDA method [18], a set of hypotheses are generated from the mean and covariance of $\{\hat{\bar{N}}^{(i)} - \hat{\bar{N}}^{(1)}\}$.
4. At each time step k, construct the residual process for each hypothesis set j under consideration.

1. From Eqs. (41) and (42), we create a random vector

$$\boldsymbol{r}_j = \begin{bmatrix} \boldsymbol{r}_{\text{carrier}_j} \\ \boldsymbol{r}_{\text{code}_j} \end{bmatrix}$$

with a known probability density function (PDF) $f_j(\cdot)$ that is independent of the states $\Delta\boldsymbol{x}$, $c\Delta t_1$, and $c\Delta t_2$. Note that if we assume that the uncertainty in $\boldsymbol{r}_j$ is a normally distributed random vector, then each $f_j[\boldsymbol{r}_j(k)]$ corresponds to a Gaussian PDF with a different mean.

5. For each set hypothesis j under consideration, define $F_j(k)$ as the probability that hypothesis set j is the correct one, given the time history of the residuals $\{\boldsymbol{r}_j(k)\}$ from time one through time k.
6. Set each of the initial values $\{F_j(0)\}$ to the equiprobable distribution $F_j(0) = 1/n$, where n is the number of hypothesis sets under consideration
7. As in [21,29], update $\{F_j(k)\}$ using the probability update rule

$$F_j(k+1) = \frac{F_j(k) \cdot f_j[\boldsymbol{r}_j(k+1)]}{\sum_{l=1}^{n} F_l(k) \cdot f_l[\boldsymbol{r}_l(k+1)]}$$

Update $\{F_j(k)\}$ using this formula until one of $\{F_j(k)\}$ exceeds the threshold T, then stop and declare the corresponding hypothesis set to be the correct one.

Note that for any given probability of the chosen hypothesis being correct, a value for T can be found that ensures that the declared hypothesis is correct with that probability. If the algorithm is allowed in principle to continue indefinitely, the Wald test minimizes the expected number of steps before a hypothesis choice is announced [29,30].

Once the wide-lane ambiguity is resolved, float L_1 frequency ambiguity N_{L_1} is estimated from the simple relationship $N_{L_2} = N_{L_1} - N_{\text{WL}}$. It follows that

$$N_{L_1} = (\lambda_1\tilde{\phi}_1 - \lambda_2\tilde{\phi}_2 + \lambda_2 N_{\text{WL}})/(-\lambda_1 + \lambda_2) \tag{43}$$

Note that the L_1 ambiguities in Eq. (43) are not integers due to the uncommon errors in phase measurements. Therefore, to find the integer values of L_1 ambiguities, the N_{L_1} hypotheses are resolved in the Wald test using the residual defined as

$$\boldsymbol{r} \triangleq N_{k,L_1} - (\lambda_1\tilde{\phi}_1 - \lambda_2\tilde{\phi}_2 + \lambda_2 N_{\text{WL}})/(-\lambda_1 + \lambda_2) \tag{44}$$

where N_{k,L_1} is the kth L_1 hypotheses.

VI. Experiments

A. Simulation

The basis for our experiments was a sequence of simulated GPS satellite positions and a sequence of simulated positions corresponding to two satellites trailing each other in the same LEO, beginning 1.1270×10^5 m apart. The trajectories of the GPS satellites were calculated from the International Global Navigation Satellite System (GNSS) Service products of 1 March 2000.[††] Simulated trajectories of the LEO satellites were generated by integrating the satellite orbit equations using a Cowell method. The LEO orbital equations included a gravitational model that used the zonal harmonics J_2 and J_3, and the 3×3 nonzonal harmonics listed in Table 1, as well as an air drag perturbation and perturbation terms accounting for the gravitational effects of the sun and moon. The orbital parameters of the LEO orbits are listed in Table 2. Note that during the simulation the LEO orbiters with the GPS receivers complete more than a half orbit, whereas the GPS satellites move less.

Both the positions of the GPS satellites and of the satellites with the GPS receivers were simulated at a 2 Hz rate. To test our algorithms, simulated GPS measurement sequences are constructed using two different measurement noise standard deviations (i.e., for both L_1 and L_2, the standard deviations for carrier-phase noise are 3 cm for one experiment and 0.3 cm for the second, and the standard deviations for C/A code noise are 3 m for one experiment and 30 cm for the second). Atmospheric distortions were added to the simulated measurements to simulate real-world conditions. Although no tropospheric distortion was added (the LEO orbits are above the troposphere), ionospheric distortion based on the Klobuchar model was imposed on the measurements [31]. During the simulation, the total electron count experienced by the GPS signals varied between a minimum of 4×10^{16} and a maximum of 1.6×10^{17}. Depending upon the parameters of each individual simulation run, measurement noise was added to the measurements to create simulated GPS signals.

Using these simulated GPS measurement sequences, we attempted to resolve the wide-lane integer ambiguities first and then, we find L_1 integer ambiguities using the resolved wide-lane integer ambiguities. Using double-differenced L_1 carrier-phase measurements in the UKF, the relative positions are estimated. These relative positioning estimates are compared with exact values.

Table 1 Gravitational coefficients used in computing LEO orbits

Coefficient	Value	Coefficient	Value
J_2	0.1082625×10^2	J_3	-2.532600×10^{-6}
C_{21}	0	S_{21}	0
C_{22}	1.5747×10^{-6}	S_{22}	-0.9024×10^{-6}
C_{31}	2.1908×10^{-6}	S_{31}	-0.2709×10^{-6}
C_{32}	0.3097×10^{-6}	S_{32}	-0.2212×10^{-6}
C_{33}	0.1001×10^{-6}	S_{33}	0.1973×10^{-6}

Table 2 Orbit parameters of LEO satellites

Parameters	Value
Semimajor axis, km	7054.1874
Eccentricity	0.0005414
Inclination, deg	98.130
R. A. of ascending node, deg	81.107
Argument of perigee, deg	270.357
Mean anomaly	179.839

B. Integer Ambiguity Resolution Test Results

When mutually observed satellites would drop into or out of view during a Wald test, the set of hypotheses for the integer ambiguities would change. This additional dynamic made it harder to compare the speed and effectiveness of the ambiguity resolution methods, depending on exactly when during a test the dropouts would occur. Fortunately, there was a sequence of 775 consecutive GPS measurement epochs within the simulated data sequence that had no changes in the GPS satellites that were mutually observed by both receivers. Our integer resolution tests were based on the simulation data from within this interval.

This satellite simulation data sequence was then broken into sequential testing periods, each testing period beginning one measurement epoch after its predecessor and ending one measurement epoch later. To illustrate this, consider the following: If we were reasonably sure that a floating-point valued estimate of the double-differenced wide-lane carrier-phase ambiguity could be generated within 50 epochs, and if we were also reasonably sure that a Wald test could determine the wide-lane integer ambiguities from a set of integer hypotheses created using the LAMBDA method applied to the float estimate within 50 epochs, then we would make each testing period 100 epochs long for the wide-lane ambiguity resolving process. After we are assured that the wide-lane ambiguities are resolved correctly, we begin searching for the L_1 ambiguities. Because L_1 float estimates from the wide-lane ambiguity are much more precise than the original wide-lane float estimates, only 5 epochs of an averaging period produces a small

[††]"International GNSS Service" [Retrieved 01 March 2000], http://igscb.jpl.nasa.gov/.

Table 3 Integer resolution results (100 Monte Carlo trials)

Measured noise	Measured frequency	Avg. no. hypotheses	Avg. convergence time	No. wrong convergences
3 m, 0.3 m	wide-lane	3250	130.3 s[a]	0
3 m, 0.3 m	L_1	68	25.2 s	0
30 cm, 0.3 cm	wide-lane	3250	23.9 s[b]	0
30 cm, 0.3 cm	L_1	40	2.7 sec.	0

[a]Includes 50 s of float estimation and mean duration of Wald test at 2 Hz sample rate.
[b]Includes 5 s of float estimation and mean duration of Wald test at 2 Hz sample rate.

number of hypotheses from the LAMBDA method, and the Wald test converges to correct L_1 ambiguities in around 6 epochs. In the first testing period, the simulated receiver positions between epoch 1 and epoch 155 would be used to generate a sequence of exact ranges from the GPS satellites to the receivers. For the second testing period, the simulated receiver positions between epoch 2 and epoch 156 would be used to generate a sequence of exact ranges from the GPS satellites to the receivers, and so forth. In this way, we could create short sequences of simulated ranges that traversed the possible positions generated in the same satellite simulation.

For each testing period, the challenge was to successfully determine the correct integers to within a given probability threshold using the filtering algorithm from Sec. IV and the Wald test algorithm from Sec. V. To simulate GPS measurements, the exact ranges between the GPS receivers and the GPS satellites in the satellite constellation simulation were corrupted by adding random biases at each receiver (to simulate the random receiver clock biases $c\Delta t_1$ and $c\Delta t_2$) and zero-mean pseudorandom sequences (to simulate the effects of the noise sequences $\{\eta_1^{(i)}(k)\}$ and $\{\eta_{12}^{(i)}(k)\}$. From the sequences of true range, ionospheric distortion, measurement noise, and clock biases provided by the simulation, we generated six simulated measurement sequences. Two of these sequences represented the C/A code pseudoranges at both receivers. Two more simulated the carrier-phase measurement at the L_1 frequency [32]. The last two represented the carrier-phase measurements at the L_2 frequency [32].

We simulate both L_1 and L_2 carrier-phase measurements to construct the wide-lane carrier-phase measurements [33]. Recall that the ratio of the wide-lane wavelength to the noise level of a wide-lane measurement is smaller than the corresponding ratio for single-frequency measurements. Although this fact along with the effective increase in the wavelength allows wide-lane integer ambiguities to be resolved more easily than single-frequency integer ambiguities, the long wavelength and amplified errors due to combining the two frequencies corrupts the positioning accuracy. Therefore, we propose the following two-step integer search process: first, resolve the wide-lane integers and then use them to resolve the L_1 integer ambiguities.

The process of integer resolution for each simulation run began by generating crude estimates of the positions of the receivers and of the clock biases using universally convergent techniques applied to the C/A code measurements of the first three simulated epochs [6,10,12]. Estimates of the velocities of the receivers and of the clock bias drift rates were then constructed by taking a central difference of the initial position estimates of the receivers. An alternate approach might be to use Doppler shift measurements in a pointlike solution for the velocity components and the clock frequency errors. The estimates of the carrier-phase ambiguities were initialized to values of $(\tilde{\rho}_2^{(i)} - \tilde{\rho}_1^{(i)})/\lambda_{\mathrm{WL}} - (\tilde{\phi}_2^{(i)} - \tilde{\phi}_2^{(i)})$, $i = 1, 2, \ldots, m$. Because these initial estimates of the carrier-phase ambiguities were very crude, they were each assigned an initial error covariance of 10^{12}.

Having thus constructed an initial state estimate, the measurements were then processed using a square-root version of the unscented Kalman filter described in Sec. IV.C for a set period that was experimentally determined to be long enough for the candidate set produced by the LAMBDA method to be sufficiently small (less than 8,000 candidate vectors on average) [28]. Then, the resulting floating-point estimate $\hat{\mathbf{x}}$ was processed to determine the integer ambiguity. The value of the first carrier-phase ambiguity estimate $\hat{\tilde{\mathbf{N}}}^{(1)}$ was then subtracted from every element of the carrier-phase ambiguity vector $\hat{\tilde{\boldsymbol{N}}}$ to generate a $(m-1)\times 1$ vector corresponding to the double-differenced carrier-phase ambiguities:

$$\hat{\boldsymbol{N}} \triangleq \left[\hat{\tilde{\mathbf{N}}}^{(2)} - \hat{\tilde{\mathbf{N}}}^{(1)}, \hat{\tilde{\mathbf{N}}}^{(3)} - \hat{\tilde{\mathbf{N}}}^{(1)}, \cdots, \hat{\tilde{\mathbf{N}}}^{(m)} - \hat{\tilde{\mathbf{N}}}^{(1)}\right]^T \tag{45}$$

By applying the LAMBDA method to $\hat{\boldsymbol{N}}$ and its variance, we then generated a set of integer ambiguity candidates that were processed using the Wald test algorithm described in Sec. V to determine the integer ambiguities. Note that once the Wald test algorithm had begun, the UKF that estimates the floating-point solution had to continue running at every measurement epoch, because the geometry of the satellite formation (and thus the values of the measurement residuals) can change significantly during the time that it takes to resolve the integers.

In Table 3, the results are summarized for several experiments in resolving the wide-lane and L_1 integers under varying amounts of simulated measurement noise, and list the number of simulations in each Monte Carlo. Although Table 3 lists the values of the simulated measurement noise, these values do not include the effects of the ionospheric biases. This may explain why the wide-lane cases have similar convergence. To account for the additional uncertainty imposed by the ionospheric biases, the assumed noise levels for the measurements (not the actual noise levels of the measurements) were tripled when the Wald tests were conducted. We can also see from Table 3 that for every sample in the Monte Carlo, the Wald test always resolved the correct integer ambiguity for both wide lane and L_1.

Figures 1 and 2 demonstrate how the probabilities $\{F_i\}$ evolve in the course of resolving the wide-lane integer ambiguity for a single simulation (in this particular simulation, there were 3556 candidate hypotheses that had a Chi-squared cost below 5000). It is clear from these figures that the probabilities $\{F_i\}$ do not evolve in a monotonic fashion. This is entirely understandable, because otherwise an

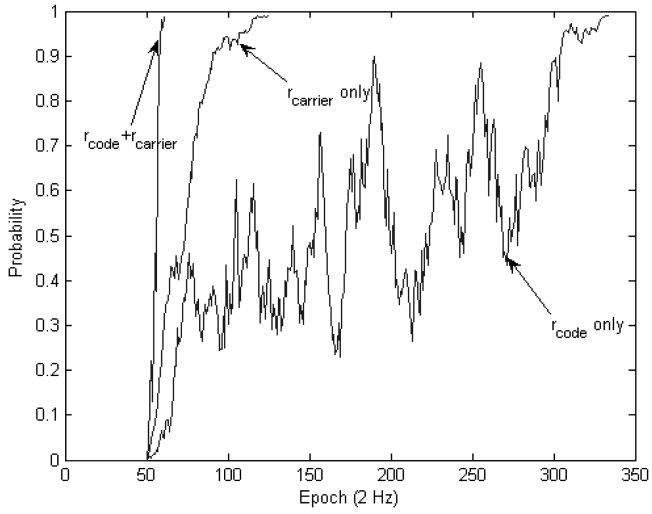

Fig. 1 Comparison of the converging time between different residuals. (includes 25 s of float estimation).

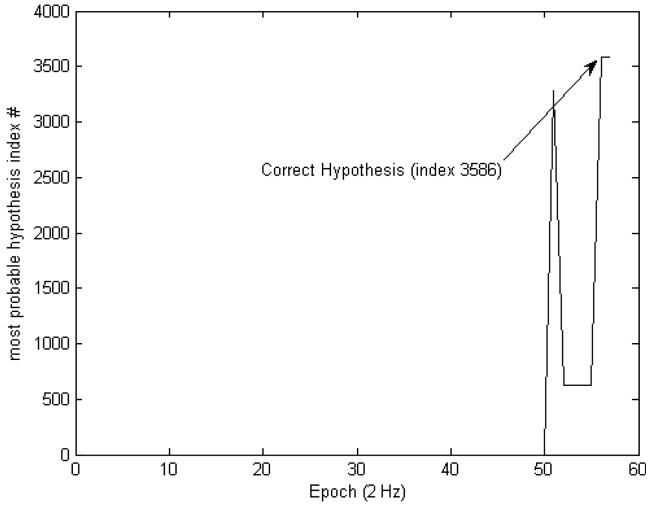

Fig. 2 Most probable hypothesis index number vs time.

increase in the probability of a wrong hypothesis due to an excursion of a few data samples could never be corrected.

C. Estimation Results

We then evaluated the effectiveness of our estimation methods using the full 3600 s long set of simulated GPS satellite and GPS receiver positions. We began by creating sequences of clock biases $\{c\Delta t_1\}$ and $\{c\Delta t_2\}$ as normally distributed zero-mean random variables with a standard deviation of 10^5 m. The clock bias sequences were then added to the sequence of true ranges to create simulated GPS pseudomeasurements. At this stage, we assumed that the integer biases $\{N^{(i)}\}$, $i = 2, 3, \ldots, m$ had been correctly determined by our integer resolution technique. At each time sample, zero-mean pseudorandom noise was added to the simulated pseudoranges, in the same way as described in the preceding section. It is assumed that the noise sequences $\mathbf{n}_1$ and $\boldsymbol{\eta}_d$ were zero-mean, independent, identically distributed random variables whose standard deviations are σ_1 and σ_d, respectively, for each measurement. Once the double-differenced ambiguities for the wide-lane and L_1 are resolved, the ionospheric delay error can be mitigated by considering double-differenced measurements between GPS satellites from Eq. (7) for L_1 and L_2 carrier-phase frequencies as

$$\lambda_k\left(\nabla\triangle\tilde{\phi}^{(i)}_{j,L_k} + \nabla\triangle N^{(i)}_{j,L_k}\right) = \nabla\delta\tilde{\rho}^{(i)}_{L_k} + \nabla\triangle I^{(i)}_{j,L_k} + \nabla\triangle\eta^{(i)}_{L_k},$$
$$i = 1, 2, \ldots, m-1, \quad j = 1, 2 \quad k = 1, 2$$

where $\nabla\triangle$ is a double-difference operation, and $\nabla\delta\tilde{\rho}$ is the double-differenced carrier phase measurements, $N_{L_2} = N_{L_1} - N_{\mathrm{WL}}$, $I_{L_2} = I_{L_1}(f_1^2/f_2^2)$. By combining the L_1 and L_2 carrier-phase measurements, the ionospheric delay error observable can be estimated from

Table 4 Estimation results: GPS C/A code noise has 3 m standard deviation, GPS L_1 and L_2 carrier noises each have 3 cm standard deviation

Ambiguity used	RMS eror, cm			Mean eror, cm		
	Radial	Along	Cross	Radial	Along	Cross
Wide-lane[a]	32.58	43.35	21.02	11.05	-3.716	-3.824
Float L_1[a]	8.048	19.49	5.80	3.684	-6.951	-4.915
Integer L_1[a,c]	4.036	7.193	2.757	-6.128	-0.882	0.620
Wide-lane[b]	4.578	2.322	1.609	12.43	-0.323	-1.516
Float L_1[b]	8.294	14.90	5.620	2.953	1.896	1.282
Integer L_1[b,c]	0.835	2.112	0.951	0.318	-0.382	-0.109

[a]3 m, 0.3 m noise [b]3 cm, 0.3 cm noise [c]Ionosphere delay error corrected

$$\left(1 + \frac{f_1^2}{f_2^2}\right)I_1^{(i)} \approx \lambda_2\tilde{\phi}^{(i)}_{j,L_2} - \lambda_1\tilde{\phi}^{(i)}_{j,L_1} + \lambda_1 N_1 - (\lambda_2 N_1 - \lambda_2 N_{\mathrm{WL}})$$

This estimate is used in Eq. (7) to remove the ionospheric delay error. Then, the relative position estimates are determined from the UKF using the enhanced double-differenced L_1 carrier-phase measurements. The positioning results are compared to the known relative positions at every measurement epoch of the simulation. Note that these nonlinear measurements are used directly in the UKF and not linearized. The results of positioning from the L_1 frequency measurement equation are tabulated in Table 4.

VII. Conclusions

We have demonstrated techniques for accurately estimating the relative positions of two widely separated satellites in Earth orbit using differential carrier-phase GPS. These included a representation of the GPS measurement equations that restricted geometric nonlinearities to a one-dimensional subspace and a universal linearization in the remaining $m-1$ dimensional subspace for both code and differential carrier-phase measurements, a UKF that generated accurate float estimates of the carrier-phase ambiguities, and a sequential hypothesis test that resolves the integer ambiguities in minimum time. Once the double-differenced wide-lane integers are resolved, the double-differenced L_1 integers are resolved allowing the L_1 carrier-phase measurements to be used in the UKF to produce accurate differential position estimates.

Acknowledgment

This research was supported in part by NASA Goddard Space Flight Center under grant NAG5-726.

References

[1] Leitner, J., Bauer, F., Folta, D., Moreau, M., Carpenter, R., and How, J., "Formation Flight in Space." *GPS World*, Vol. 13, No. 2, 2002, pp. 22–31.

[2] Kroes, R., Montenbruck, O., Bertiger, W., and Visser, P., "Precise GRACE baseline determination using GPS," *GPS Solutions*, Vol. 9, No. 1, April 2005, pp. 21–31.

[3] Haines, B., Bertiger, W., Desai, S., Kuang, D., Munson, T., Young, L., and Willis, P., "Initial Orbit Determination Results for Jason-1: Towards a 1 cm Orbit," *Navigation: Journal of the Institute of Navigation*, Vol. 50, No. 3, 2003, pp. 171–180.

[4] Zhu, S., Reigber, C., and König, R., "Integrated Adjustment of CHAMP, GRACE, and GPS Data," *Journal of Geodesy*, Vol. 78, Nos. 1–2, Sept. 2004, pp. 103–108.

[5] Leung, S., and Montenbuck, O., "Real-Time Navigation of Formation-Flying Spacecraft Using Global-Positioning-System Measurements," *Journal of Guidance, Control, and Dynamics*, Vol. 28, No. 2, 2005, pp. 226–235.

[6] Bancroft, S., "Algebraic Solution of the GPS Equations," *IEEE Transactions on Aerospace and Electronic Systems*, Vol. AES-21, No. 1, 1985, pp. 56–59.

[7] Abel, J. S., and Chaffee, J. W., "Existence and Uniqueness of GPS Equations," *IEEE Transactions on Aerospace and Electronic Systems*, Vol. AES-27, No. 6, 1991, pp. 952–6.

[8] Chaffee, J. W., and Abel, J. S., "On the Exact Solutions of Pseudorange Equations," *IEEE Transactions on Aerospace and Electronic Systems*, Vol. AES-30, No. 4, 1994, pp. 1021–30.

[9] Leva, J. L., "Alternative Closed-Form Solution to the GPS Pseudo-Range Equations," *IEEE Transactions on Aerospace and Electronic Systems*, Vol. 32, No. 4, 1996, pp. 1430–9.

[10] Biton, I., Koifman, M., and Bar-Itzhack, I. Y., "Improved Direct Solution of the Global Positioning System Equation," *Journal of Guidance, Control, and Dynamics*, Vol. 21, No. 1, 1998, pp. 45–49.

[11] Pachter, M., and Nguyen, T. Q., "Efficient GPS Position Determination Algorithm," *Navigation: Journal of the Institute of Navigation*, Vol. 50, No. 2, 2003, pp. 131–141.

[12] Wolfe, J. D., and Speyer, J. L., "Universally Convergent Statistical Solution of Pseudorange Equations," *Navigation: Journal of the Institute of Navigation*, Vol. 49, No. 4, 2002, pp. 183–192.

[13] Spilker, J. J., Jr., "Tropospheric Effects on GPS," *Global Positioning System: Theory and Applications*, edited by B. W. Parkinson and J. J.

Spilker Jr., Vol. 1, AIAA, Washington, D.C., 1996.
[14] Bassiri, S., and Hajj, G. A., "Higher-Order Ionospheric Effects on the Global Positioning System Observables and Means of Modelling Them," *Manuscripta Geodaetica*, Vol. 18, No. 5, Sept. 1993, pp. 280–289.
[15] Gu, M., and Brunner, F. K., "Theory of the Two Frequency Dispersive Range Correction," *Manuscripta Geodaetica*, Vol. 15, No. 6, Dec. 1990, pp. 357–361.
[16] Blewitt, G., "Carrier Phase Ambiguity Resolution for the Global Positioning System Applied to Geodetic Baselines up to 2000 km," *Journal of Geophysical Research*, Vol. 94, No. B8, 1989, pp. 10,187–10,203.
[17] Spilker, J. J., Jr., "Foliage Attenuation for Land Mobile Users," *Global Positioning System: Theory and Applications*, edited by B. W. Parkinson and J. J. Spilker Jr., Vol. 1, AIAA, Washington, D.C., 1996.
[18] Teunissen, P. J. G., "New Method for Fast Carrier Phase Ambiguity Estimation," *IEEE 1994 Position Location and Navigation Symposium*, Inst. of Electrical and Electronics Engineers, New York, 1994, pp. 562–73.
[19] Hassibi, A., and Boyd, S., "Integer Parameter Estimation in Linear Models with Applications to GPS," *IEEE Transactions on Signal Processing*. Vol. 46, No. 11, 1998, pp. 2938–2952.
[20] Xu, P., "Random Simulation and GPS Decorrelation," *Journal of Geodesy*, Vol. 75, No. 7, 2001, pp. 408–423.
[21] Wolfe, J. D., Williamson, W. R., and Speyer, J. L., "Hypothesis Testing for Resolving Integer Ambiguity in GPS," *Navigation: Journal of the Institute of Navigation*, Vol. 50, No. 1, 2003, pp. 45–56.
[22] Jazwinski, A. M., *Stochastic Processes and Filtering Theory*, Academic, New York, 1970.
[23] Schutz, B. E., Tapley, B. D., Abusali, P. A. M., and Rim, H. J., "Dynamic Orbit Determination Using GPS Measurements from TOPEX/POSEIDON," *Geophysical Research Letters*, Vol. 21, No. 19, 1994, pp. 2179–2182.
[24] Julier, S. J., Uhlmann, J. K., and Durrant-Whyte, H., "New Approach for Filtering Nonlinear Systems," *Proceedings of the American Control Conference*, Vol. 3, Inst. of Electrical and Electronics Engineers, New York, 1995, pp. 1628–1632.
[25] Ito, K., and Xiong, K., "Gaussian Filters for Nonlinear Filtering Problems," *IEEE Transactions on Automatic Control*, Vol. 45, No. 5, 2001, pp. 910–927.
[26] Arulampalam, M. S., Maskell, S., Gordon, N., and Clapp, T., "Tutorial on Particle Filters for Online Nonlinear/Non-Gaussian Bayesian Tracking," *IEEE Transactions on Signal Processing*, Vol. 50, No. 2, 2002, pp. 174–188.
[27] Julier, S. J., and Uhlmann, J. K., "Unscented Filtering and Nonlinear Estimation," *Proceedings of the IEEE*, Vol. 92, No. 3, 2004, pp. 401–422.
[28] van der Merwe, R., and Wan, E. A., "Square-Root Unscented Kalman Filter for State and Parameter Estimation," *2001 IEEE International Conference on Acoustics, Speech, and Signal Processing*, Vol. 6, Inst. of Electrical and Electronics Engineers, Piscataway, NJ, May 2001, pp. 3461–4.
[29] Malladi, D. P., and Speyer, J. L., "Generalized Shiryayev Sequential Probability Ratio Test for Change Detection and Isolation," *IEEE Transactions on Automatic Control*, Vol. 44, No. 8, 1999, pp. 1522–34.
[30] Wald, A., *Sequential Analysis*, Wiley Mathematical Statistics Series, Wiley, New York, 1947.
[31] Klobuchar, J. A., "Ionospheric Effects on GPS," *Global Positioning System: Theory and Applications*, edited by B. W. Parkinson and J. J. Spilker Jr., Vol. 1, AIAA, Washington, D.C., 1996.
[32] Spilker, J. J., Jr., "GPS Signal Structure and Theoretical Performance," *Global Positioning System: Theory and Applications*, edited by B. W. Parkinson and J. J. Spilker Jr., Vol. 1, AIAA, Washington, D.C., 1996.
[33] Goad, C., "Surveying with the Global Positioning System," *Global Positioning System: Theory and Applications*, edited by B. W. Parkinson and J. J. Spilker Jr., Vol. 2, AIAA, Washington, D.C., 1996.